Heat Transfer Study in a Rotor Stator System Air Gap with an Axial Inflow

Julien Pellé, Souad Harmand

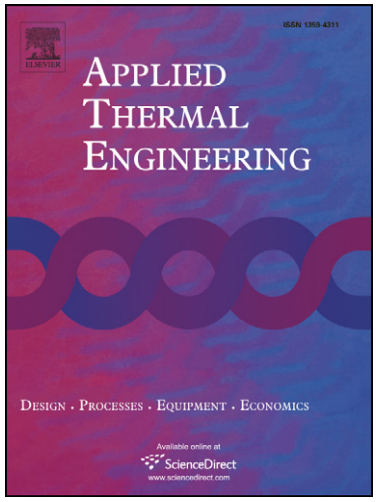

Heat Transfer Study in a Rotor Stator System Air Gap with an Axial Inflow

Julien Pellé, Souad Harmand

PII: S1359-4311(08)00304-9
DOI: 10.1016/j.applthermaleng.2008.07.014
Reference: ATE 2567

To appear in: *Applied Thermal Engineering*

Received Date: 6 June 2007
Revised Date: 12 June 2008
Accepted Date: 7 July 2008

Please cite this article as: J. Pellé, S. Harmand, Heat Transfer Study in a Rotor Stator System Air Gap with an Axial Inflow, *Applied Thermal Engineering* (2008), doi: 10.1016/j.applthermaleng.2008.07.014

Heat Transfer Study in a Rotor Stator System Air Gap with an Axial Inflow

Julien Pellé *, Souad Harmand

Laboratoire de Mécanique et Energétique
Université de Valenciennes et du Hainaut-Cambrésis
Le Mont Houy
59313 Valenciennes CEDEX 9 – FRANCE

Abstract

Discoidal rotor-stator systems are nowadays sometimes used in electrical wind generator. The cooling of such a system is a major problem due to the fact that high electrical losses are dissipated for relatively low rotational speed, responsible of the cooling. A new cooling solution is then investigated in this paper. So, this article presents an experimental study of the local heat transfers on the rotor surface in the air-gap of a discoidal rotor-stator system, in which an air jet comes through the stator and impinges the rotor. To determine the surface temperatures, measurements were taken on the rotor, using an experimental technique based on infrared thermography. A thermal balance equation was used to identify the local convective heat transfer coefficient. The influence of the axial Reynolds number Re_j and the rotational Reynolds number Re was measured and compared with the data available in the literature. Local convective heat transfer coefficients were obtained for an inter-disk dimensionless spacing interval G ranging from 0.01 to 0.16 for Re_j between 0 and 41666 and for Re between 20000 and 516000. The rotating disk can thus be divided into zones: one dominated by the air jet near the center of the rotor and one affected by both the air jet and rotation. Even though these two zones are not located in the same place on the disk, the heat transfers with non-zero impinging jets appear to be continuously improved compared to those with no jets. Critical radii over the rotor surface are identified and correlations are given.

Key words: Rotor-Stator, Infrared thermography, Convective heat transfer, Impinging jet, Discoidal electrical machines

* Corresponding Author: Fax 00 33 327 511 961
Email address: jpelle@univ-valenciennes.fr (Julien Pellé).

Nomenclature

x	Axial Position, m
r	Radius, m
R_{ext}	Outer radius of rotor, m
k	Thermal conductivity, W.m^{-1}.K^{-1}
h	Convective heat transfer coefficient, W.m^{-2}.K^{-1}
$\overline{h}$	Mean convective heat transfer coefficient, W.m^{-2}.K^{-1}
T	Temperature inside zircon, K
T_s	Disk surface temperature, K
T_∞	Atmospheric temperature, K

Greek Symbols

ϵ_r	Rotor Emissivity
ϵ_s	Stator Emissivity
τ	Air Transmission coefficient
τ_f	Fluorspar window Transmission coefficient
ω	Rotational Speed, rad.s^{-1}
λ	Flow parameter
ϕ	Heat flux W.m^{-2}
θ	Temperature difference $T_s(r) - T_\infty$, K

Subscripts and Superscripts

cv	Convection
cd	Conduction
ray	Radiation
lam	Laminar flow
tr	Transition
$turb$	Turbulent flow

Dimensionless Numbers

C_w	= Mass Flow rate coefficient
G	= Dimensionless Spacing
Re_r	= Local Reynolds number
Re	= Rotational Reynolds number

Re_j = Jet Reynolds number
Nu_r = Local Nusselt number
$\overline{Nu}$ = Mean Nusselt number

1 Introduction

Nowadays, the power production industry is confronted with new challenges due to the need for sustainable development. For example, studies about wind generators have become more and more numerous. In order to decrease the costs of such wind systems, more energy must be produced per aerogenerator. Industry has worked to increase power production by attempting to increase generator efficiency. Industrialists have become involved in the development of discoidal rotor-stator systems. These systems don't use gears in order avoid altering the system's mechanical efficiency, and are thus able to produce a lot of power at low rotational speeds. For example, the reference case for this study is a wind generator which have been situated in the north of France. It can deliver 750kW for a maximal rotational speed of 25 rpm. However, the increased production leads to inefficient cooling, generally only due to the effect of rotation. Knowledge of the parameters that influence the convective heat transfer in the air gap can help manufacturers to avoid overheating. In our study, an impinging jet, passing through the center of the stator and coming into direct contact with rotor, was added in order to improve the motor's cooling method.

2 Literature review

2.1 Generalities about rotating disks

Von Karman [1]was the first author to describe the air flow around a rotating disk. There are two significant velocity components inside that boundary layer: the first one is radial, highlighting the effect of inertia due to the rotation, and the second is tangential, highlighting the effect of air viscosity. The convective heat transfers on a rotating disk have also been studied by Goldstein [2], Cobb et Saunders [3] and Richardson et Saunders [4] and Dorfman [5]. Dorfman [5] has suggested many correlations for both local and mean Nusselt numbers, taking the radial temperature profile of the disk surface into account. More recently, Cardone [6] has proposed a correlation in the case of a transitional flow from laminar to turbulent.

Several authors have also studied the influence of jet impingement, for example, Huang [7], who worked with different jet generators, or Fenot [8], who worked with several simultaneous jets. Angioletti et al. [9] have concluded that shear stress and, consequently, heat transfer increase when the boundary layer near the surface is perturbed and the accelerated air is renewed. Other authors have studied mass and heat transfer changes in a single rotating disk configuration. Chen et al. [10], Owen and Rogers [11] and Astarita [12] have examined the sensitivity of Nusselt numbers to jet diameter D, to the jet's Reynolds number Re_j, and to the distance between the jet outlet and the disk e/D. In the case of a discoidal rotor-stator system without a jet impingement, the flow structure was also studied by few authors as Soong [13] or Poncet [14]. Beretta [15] has completed those studies by determining the convective heat transfer.

Absent from this general information is any reference to a study of the influence of jet impingement on the heat transfers in a discoidal rotor-stator system. Only a study of the convective heat transfer without any impinging jet is available and have been done by Pellé and Harmand [16], previously to the present study. Concluding that this subject has not been yet studied, we decided to examine the effect of an air jet on the cooling of a rotating disk in a discoidal rotor-stator system. Owen and Rogers [11] have studied the air flows in such a configuration, and their results were quite useful for positioning our results. The next section provides a brief description of their research about the air flow in the air gap between the two face-to-face disks.

2.2 Rotor-stator configuration with an axial flow

For the wind generator that has been chosen for this study, the rotor diameter is about 3 meter and the air gap thickness is about 15 mm. With its maximal speed of 25 rpm, the Reynolds number reaches a maximal value of about 4×10^5, which can produce both laminar or turbulent flow, and the dimensionless spacing G is about 0.01, which can be considered as a narrow dimensionless spacing interval. That configuration produces a poor quality of cooling and the addition of a jet is investigated in terms of cooling improvement. In order to better understand the cooling mechanism with the addition of a jet impingement, some literature data are exposed thereafter.

Owen and Rogers [11] have studied the effect of modifying the flow inside the air gap for different dimensionless spacing intervals G. They identify four possible flow configurations, depending on the Reynolds number and on the dimensionless spacing interval. However, the limits between those domains are not quantitatively defined. In these configurations, the flow can be either laminar or turbulent and the spacing interval between the two disks can be either narrow or wide.

2.2.1 Configuration I

In the case of a narrow dimensionless spacing interval and a laminar flow, the flow structure depends on the diameter of the opening and the injected mass flow rate. Soo [17] has solved Navier-Stokes equations theoretically, and he showed that the flow structure depends on a parameter, such as:

$$\Phi(\tilde{r}) = \frac{G\, C_W}{2\pi \times (Re_G\, \tilde{r})^2} \tag{1}$$

where $Re_G = \frac{\omega r e}{\nu}$ and $\tilde{r} = \frac{r}{R_{ext}}$. If there is no opening in the center of the stator, this parameter is null, and the flow is centrifugal near the rotor and centripetal near the stator. The boundary layers are merged, and the flow is a Couette-type flow. For Soo [17], when $\Phi(\tilde{r}) < 0.01$, the flow conforms to the above description. In the other cases, the flow is centrifugal across the entire width of the air-gap. When a flow enters the air-gap via the opening in the stator, the appearance radius of the centripetal flow increases, compared to a configuration without an axial inflow. The boundary layer near the rotor is partially supplied by the flow entering the stator, instead of being completely supplied by the centripetal flow near the stator. In fact, given a significant injected mass flow rate, this centripetal flow can be totally absent from the air-gap.

2.2.2 Configuration III

In the case of a narrow spacing interval between the two disks and a turbulent flow, the flow structure is identical to the laminar case presented in configuration I by Soo [17]. When the injected flow rate is very high and the rotational velocity of the rotor very low, the flow parameter $\lambda_0 = C_W \, {Re_r}^{-0.75}$ tends toward infinity. Consequently, the local and mean heat transfers tend toward a limit, which is determined using the moment coefficient and shear stresses.

2.2.3 Configuration II

In this configuration, the spacing interval G is wide and the flow is laminar. A rotating core of fluid can thus appear inside the air-gap between the two boundary layers that develop near the disks. For a laminar flow, a parameter is also defined as:

$$\lambda_{lam} = C_W \, {Re_r}^{-0.5} \tag{2}$$

Soo [17] has shown that the tangential velocity of the rotating core of fluid is a function of $\tilde{r}$. If $\tilde{r} < \tilde{r}_0$, where $\tilde{r}_0 = \left(\frac{\lambda_{lam}}{\pi}\right)^{0.5}$, the rotating core of fluid does not appear in the air-gap, and the flow near the rotor is similar to the one obtained for a single rotating disk.

2.2.4 Configuration IV

In this final configuration, the spacing interval G is again wide, but the flow is turbulent. The mean structure of the turbulent flow is similar to the previous configuration. Some authors have defined the flow parameter for this case as:

$$\lambda_{tur} = C_W \, {Re_r}^{-0.8} \tag{3}$$

In order to characterize the flow, Owen [11] has defined a parameter, such that $\tilde{r}_1 = \left(\frac{\lambda_{tur}}{0.219}\right)^{5/13}$. When $\tilde{r} < \tilde{r}_1$, the rotation of the fluid core becomes negligible, and the flow is a Stewartson-type flow [18] with boundary layers that develop near both disks that are not merged.

3 Experimental Study

3.1 Apparatus

The Reynolds analogy is used to define our experimental apparatus. The diameter of the rotating disk was 620 mm. The rotational Reynolds number could be varied between 20000 and 645000. Four infrared emitters were placed on the bottom of the disk as shown in Figure 1.

For the rotor, we chose aluminum for its high thermal conductivity (200 W/mK). An insulating material is placed at the backside of the rotor and we decided to use a layer of zircon, deposited on the aluminum via plasma projection. In order to obtain the most homogeneous temperature at the zircon/aluminum interface and the highest radial gradient on the cooling surface, we estimated the thicknesses of the two materials: the aluminum was set at 43 mm and the zircon was set at 25 mm due to the depth limitations of the plasma projection process.

An aluminum disk measuring 620 mm in diameter was chosen for the stator. It was placed at distances ranging from 3 to 50 mm, far enough from the rotor to allow an interesting range of dimensionless spacing intervals G. A window is placed in the stator to permit the observation of the rotor. We chose fluorspar for its high transmission coefficient. The rotor radii, which could be observed through this fluorspar window, ranged from 0.02 to 0.31 m. A hole ($D = 26$ mm) was pierced at the center of the stator to allow passage of a pipe linked to a centrifugal blower, which was used to impose an axial flow. The imposed axial Reynolds numbers can be varied between 8.3×10^3 and 41.6×10^3.

3.2 Procedure

3.2.1 Local Nusselt number calculation

To determine the local convective coefficients and the local Nusselt numbers, the parietal heat flux on the rotating surface must be known. This flux can be obtained by solving the Laplace equation. The zircon is meshed, and a difference-finite method is then used to solve equations. The boundary conditions applied are the surface temperatures recorded by the infrared camera and the interface temperatures recorded by the thermocouples. The local Nusselt

number is obtained:

$$Nu_r = \frac{h\,r}{k_{air}} = \frac{k\left(\frac{\partial T(r)}{\partial z}\right)_{z=0} - \sigma\frac{F\varepsilon_d\varepsilon_s}{1-F^2(1-\varepsilon_d)(1-\varepsilon_s)}\left(T_s(r)^4 - T_{stator}^4\right)}{T_s(r) - T_\infty} \times \frac{r}{k_{air}} \quad (4)$$

F is the form factor between two parallel disks as given by Ritoux [19].

3.2.2 Mean Nusselt number calculation

By integrating the local heat flux onto the rotating surface, the dissipated energy can be obtained, which can be expressed as a flux density. The mean Nusselt number can thus be expressed as:

$$\overline{Nu} = \frac{2}{R_{ext}} \times \frac{\int_0^{R_{ext}} Nu \times (T_s(r) - T_\infty)dr}{\overline{T_s(r) - T_\infty}} \quad (5)$$

3.2.3 Temperature measurements of the rotor surface

Rotor temperatures were obtained using an AGEMA 900 infrared camera. The camera observed the disk surface with a measuring frequency of 35 Hz. To increase the importance of the infrared radiative flux emitted by the rotating disk, the disk surface was painted with a high emissivity black paint. The surface emissivity was estimated by calibration, such that $\varepsilon_r = 0.93 \pm 0.01$. The fluorspar transmission coefficient is given by the manufacturer such that $\tau_f = 0.95 \pm 0.01$. For the used observation distance, it is assumed that the air transission coefficient is equal to $\tau_a = 0,95 \pm 0.01$ During a test run, the infrared camera recorded the following flux I_r:

$$I_r = \tau_f\tau_a J_r + (1-\tau_a)I(T_\infty) + \tau_a\tau_f^2(1-\epsilon_r)I_{env} \quad (6)$$

The term J_r is the rotor radiosity, which includes all the signals emitted by the rotor and all reflections coming off it. The camera also recorded this rotor radiosity, altered by the air and fluorine transmission coefficients, plus an atmospheric term $I(T_\infty)$ and an environmental term I_{env}. The atmospheric term, $I(T_\infty)$, was estimated by measuring T_∞ using a thermocouple and the calibration law. The environmental term, I_{env}, was estimated by positioning a reflecting aluminum sheet in proximity to the surface. The rotor radiosity was estimated by solving a radiosity system equation, considering the air-gap as a closed system whose boundaries are the rotor, the stator and the fluorspar window, and the crown shaped by the air. In our temperature range, $323 < T < 353$ K, the absolute error is estimated to be 1 K.

3.2.4 Temperature measurements at the zircon/aluminium interface

As shown in figure 1, two thermocouples (denoted 1 and 2)-situated inside the two holes ($D = 3$ mm) at the bottom of the disk at the aluminium/zircon interface to put them in constant contact with the zircon layer-were linked to an acquisition system by a four-channel rotating mercury ring collector passing through the shaft. They were placed at two different radii: $r = 0$ and $r = 0.3$ m. The absolute error for the aluminium/zircon interface temperature is estimated at ± 0.3 K.

3.2.5 Temperature measurement in the stator

Two T-type thermocouples-situated inside the two holes ($D = 3$ mm) at the bottom of the stator to put them in constant contact with the stator surface inside the air-gap-were directly linked to the acquisition system (numbers 3 and 4 in figure 1). They were placed at radii of 0.05 cm and 0.3 cm. The absolute error for the stator temperature is estimated at ± 0.3 K.

4 Results

This section reports the results for the convective heat transfer on the rotor of the discoidal rotor-stator system, in which there is an opening in the center of the stator. The jet diameter was set at $d = 26$ mm. The jet Reynolds number Re_j ranged from 8.3×10^3 to 41.6×10^3 and the rotational Reynolds number Re from 0.2×10^5 to 5.16×10^5. The dimensionless spacing interval G varied between 0.01 and 0.16. When possible, our results are compared with the results obtained using $Re_j = 0$.

4.1 Local Nusselt numbers

4.1.1 Generalities

Figure 2 show a representation of the phenomena at the rotor surface, according to many authors and to the results explained thereafter for a better understanding.

As many authors have observed, the presence of an impinging jet increases the local heat transfer values, compared to the values obtained without jet impingement (when $Re_j = 0$). As the injected mass flow rate increases, the values become even higher, which can be explained by a larger quantity of

renewed air inside the air-gap. Figures 3 and 5 show the local Nusselt number profiles for a fixed jet Reynolds number. These figures show that there is an area near the center of the rotating disk, where heat transfers do not depend on rotational velocity, which confirms the observations of both Chen and Popiel [10,20]. The size of this area depends on the dimensionless spacing interval G, because it increases when G increases. Figures 4 and 6 show the local Nusselt number profiles for a constant rotational velocity. It appears that all the profiles tend toward the same limit, highlighting the fact that, for outer radii, there is an area where the convective heat transfer does not depend on the jet Reynolds number. Although the area shown in the first set of figures is always present on the rotating disk, the area shown in the second set of figures only appears under suitable conditions of G, Re and Re_j. For example, when G or Re becomes higher, for a fixed Re_j, it is easier to get an area on the rotating disk where the convective heat transfer does not depend on the jet Reynolds number. In fact, the jet effect is significant near the stagnation point, and due to the axisymetry of the system, its influence diminishes as r increases. On the other hand, the rotational influence is more significant at the outer radii, due to the effect of viscosity. Therefore, it appears that there is a point at which the effect of rotation becomes more significant than the effect of the jet.

The following sub-sections provide our detailed observations of the local Nusselt numbers for three of the five studied dimensionless spacing intervals G.

4.1.2 G=0.16

For this wide spacing configuration, the results are very similar to those obtained by Popiel and Boguslawski [20] for a single rotating disk with an impinging jet.

For a constant Re_j, on Figure 3, the results do not depend on Re, the rotational Reynolds number, in the central area of the disk surface. At higher radii, values vary with Re, which demonstrates the decrease in the jet's influence. At this point, the local Nusselt numbers are higher when the rotational velocity increases. In addition, the higher the injected mass flow rate, the higher the dimensionless radii at which the local Nusselt number profiles become different.

For a constant Re, on Figure 4, the size of central area, where an increase in the convective heat transfer can be observed, is significant. Near the air-gap outlet, as mentioned previously, the different local Nusselt number profiles tend toward the same limit, which means the jet loses influence as the effect of rotation becomes more important. In fact, the local Nusselt number profile

tends toward the value obtained without an impinging jet, which is clearly visible when $Re = 5.16 \times 10^5$. However, an inversion can also be noted: at outer radii, the highest injected mass flow rates produce the lowest convective heat transfers. For other values of Re, this tendency is less marked. Nonetheless, the inversion is almost always noticeable, only disappearing at the lowest experimental Re_j values.

4.1.3 G=0.01

It can be noticed again that the Nu_r is not very dependant with r/D at low radii on Figure 5. Local Nusselt numbers vary significantly with Re_j, whatever Re (Figure 6) but vary less with the radius (Maximal variation of 250 over the disk against 550 when $G = 0.16$), which reflects the fact that the shear stress between the air and the rotor surface does not vary a lot.

4.1.4 Synthesis

All the previous observations demonstrated how the parameters G, Re and Re_j influence the local convective heat transfer on a rotating disk. In summary, it appears that:

- With fixed G and Re_j values, an increase in Re leads to an increase in the local Nusselt number for outer radii, although for the lowest radii, the rotational speed does not influence the local Nusselt number.
- With fixed G and Re values, an increase in Re_j leads to a significant increase in the local convective heat transfers near the stagnation point; however, a decrease in the heat transfer can be observed at outer radii near the air-gap outlet.
- With fixed Re and Re_j values, an increase in G leads to an increase in the size of the central area where the jet influence is greatest.

4.2 Mean Nusselt numbers

The evolution of the mean Nusselt numbers is studied by varying the three parameters: G, Re and Re_j. In addition to modifying these parameters, it is also interesting to see how the mean Nusselt numbers change when a jet is added to the configuration, compared to the configuration without a jet. Figure 7 present five charts, corresponding to the five different G values. These charts show the evolution of the mean Nusselt number versus Re for each Re_j values.

4.2.1 Influence of the injected mass flow rate Re_j

Globally, an increase in the injected mass flow rate leads to an increase in the global heat transfer. The charts also show that, whatever the Re value, the first derivative of $\overline{Nu}$ is quite similar for a fixed dimensionless spacing interval G but quite different for changing values of G. The variation in the spacing interval discussed in the next sub-section is thus of interest.

4.2.2 Influence of the dimensionless spacing G

For the no-jet case [16], the mean Nusselt numbers are low at low G values and increase with G until reaching the same limits as the ones for a rotating disk in still air, depending on Re. Increasing the injected mass flow rate significantly increases the mean Nusselt numbers at low G values, and they continue to increase as G increases. Furthermore, the mean Nusselt number gradient is higher when Re_j is higher, and the mean Nusselt numbers no longer tend noticeably toward a limit as in the no-jet case. However, for a sufficiently high G value, these values obviously tend toward the same limit as the case with one jet. This tendency does not appear in our results because our maximum G value is too low for the influence of the jet to be decreased enough to appear. In fact, for this limit to be apparent, both the injected mass flow rate and the dimensionless spacing interval must be fairly high. Since differences in the mean Nusselt numbers are observed when the rotational speed is changed, the next sub-section deals with the influence of Re on mean Nusselt numbers.

4.2.3 Influence of the rotational speed Re

$\overline{Nu}$ is an increasing function of Re if Re is high enough, except when $G = 0.01$. Indeed, several of the profiles show that $\overline{Nu}$ does not depend on Re if $Re < 2 \times 10^5$, namely when $G = 0.16$ and Re_j is at its highest level. Chen [21] made the same observation about the global convective heat exchange over the entire surface of a single rotating disk subjected to an impinging flow. In addition, according to these charts, the slopes are higher when G is high. In all cases, the profiles are similar to the no-jet case [16] when $Re > 2 \times 10^5$. Only the vertical offset remains, which is higher for a high injected flow rate.

4.3 Interpretation

4.3.1 Convective heat transfers

The local Nusselt number profiles make it possible to distinguish 3 areas on the rotor surface: in the first, the local convective heat transfers depend only on

the injected mass flow rate; in the second, the heat transfers depend on both the rotational velocity and the injected mass flow rate; and in the third, the heat transfers depend only on the rotational velocity. These zone distinctions have also been made by several authors working on jet's impinging on a flat surface. Based on our results, it is possible to determine some mathematical laws for locating the transition zone between the three areas.

In order to determine the position between zones, in each radius, the mean value of local Nusselt number was calculated for a fixed value of Re_j or Re. It gave us a mean curve of local Nusselt number, which is reported on Figure 8. Then, the radii where the difference between at least two of our experimental profiles and that mean curve exceeds 10% were recorded. Figure 8 the identified radii. The following law is proposed for the transition between the jet dominated area and the mixed area:

$$\left(\frac{r}{D}\right)_{jm} = 0.0325\,(1 - exp(-45G))\,{Re_j}^{0.5} \tag{7}$$

Since this transition zone was established based on all of the tested configurations, this law is applicable for the full range of parameter variations.

A law was also determined for the transition zone between the rotation-dependent area and the mixed dependency area. This transition zone was not observed in all cases; in fact, the rotation-dependent area only appears when the rotational velocity in the air-gap is sufficiently high. As defined, the position depends on G and Re but not on Re_j. This calculation can be divided into two parts. For the lowest dimensionless spacing intervals, $G = 0.01$, the local Nusselt numbers profiles again do not meet at outer radii. However, for larger dimensionless spacing intervals G, there is a critical local Reynolds number, Re^r_{mr}. The law is is applicable whenever $0.04 < G < 0.16$, whatever the Re or Re_j value, and expressed as follows:

$$Re^r_{mr} = 0.4\left(1 + exp(0.365\,Re \times 10^{-5})\right)\left(1 + exp(-15G)\right) \tag{8}$$

For each tested configuration, we are able to determine the limits between the zones where both the jet and rotation has influence on convective heat transfers. Figure 9 presents two examples of these boundaries.

In summary, three zones were distinguished on the disk surface by observing the local Nusselt number profiles, with the limits between the zones depending on G, Re and Re_j. However, local convective heat transfers are strongly linked to the flow inside the air-gap. The next sub-section presents a comparison with the data about this flow available in the scientific literature.

4.3.2 Flow and heat transfers similarity

As mentioned previously, with narrow spacing intervals, the local Nusselt numbers do not vary a lot over the disk surface, which is the opposite of the situation with wide intervals. The result of the $\phi(x)$ calculation shows that the flow is a centrifugal Couette-type flow, with a preponderant viscosity effect inside the air-gap. Compared to the influence of the jet, rotation does not have a preponderant influence on the local convective heat transfer. The mean Nusselt numbers, which are quite stable with a varying rotational velocity for low G values, confirm this. However, an increase in the injected mass flow rate increases the speed of the flow throughout the air-gap, due to the narrow spacing interval and the parietal stress on the rotor surface. This can also explain why the different profiles do not converge when plotting $\overline{Nu}$ at a fixed Re value.

Compared to the two radii described with equations (2) and (3), this radius, obtained from observations of the heat transfers, is located differently from the radius defined by Owen [11]. Figure 9 presents the results for the two different cases.

The boundary proposed by Owen is located between the two radii defined above. There is a strong link between the flow structure and the convective heat transfers, and the results shown in Figure 9 confirm this. Thus, it is easier to understand the observed convective heat transfers. Compared to the no-jet configuration [16], regardless of the Re and G values, the addition of an impinging jet imposes a minimal centrifugal mass flow rate inside the air-gap and significantly increases the radial velocities.

In terms of axisymetry, the jet influence is a decreasing function $(1/r)$ of the local radius, while the rotation of the air inside the air-gap is a function of $\omega\, r$. These phenomena invert as r/D increases, which explains the presence of a central area where the local convective heat transfers are determined by the jet. Since the imposed radial flow is totally centrifugal, the imposed flow rate leads to a significant increase in parietal stress on the rotor and an increase in the heat transfer. Under the influence of viscosity, the fluid progressively rotates as r/D increases. The radial flow is gradually confined near the rotor [11], and a centripetal flow appears near the stator at outer radii. The flow is thus a Batchelor-type [22] flow. The flow's confinement near the rotor increases both the parietal stress and the heat transfer in this mixed area, but less significantly than in the central area. For the higher radii, radial velocity is more influenced by rotation than by the jet, and consequently the heat transfers are very similar to those obtained without jet impingement. As in

the configuration without jet impingement [16], when G increases, tangential velocity, like the viscosity effect, is reduced and the centripetal flow tends to disappear.

The mean Nusselt numbers reflect an increase in Re_j involving an increase in the global heat transfer for all G and Re values. This is due to the increase in the local heat transfer in the central area, which also increases in size. For higher Re_j values, the centrifugal flow takes up more space in the air-gap. When the rotational velocity is high enough, $\overline{Nu}$ depends on Re, giving rise to a rotation-dominated area. Thus, since the local Nusselt numbers increase at outer radii, like in no-jet configuration, increasing Re values lead to increasing $\overline{Nu}$ values.

Previous correlated radii are reported on Figure 2 for a better understanding.

4.4 Correlations

4.4.1 Local Nusselt numbers

The influence of the jet is highlighted by a significant increase in the convective heat transfer near the central area of the rotor. Correlations are needed to provide an idea of the maximum transfer encountered and its location on the disk surface. In this central area, the effect of the rotation is negligible, thus the correlation is a function of G and Re_j. In order to best represent the measurements, the full range of the studied G values was divided into three groups: $0.01 < G < 0.02$; $0.02 < G < 0.04$ and $0.04 < G < 0.16$. The laws for the three groups are as follows:

$$Nu_{max} = 0.025\, G^{-0.1}\, Re_j^{0.85} \tag{9}$$

And for $0.02 < G < 0.04$, it is found:

$$Nu_{max} = 0.145\, G^{0.35}\, Re_j^{0.85} \tag{10}$$

Finally, For $0.04 < G < 0.16$:

$$Nu_{max} = 0.04\, G^{-0.05}\, Re_j^{0.85} \tag{11}$$

It can be seen that the Re_j power does not vary with G. Whatever the G value considered, varying the Re_j value has the same effect on the local Nusselt number. On the other hand, the influence of G changes depending on the group of G values chosen.

It is also possible to locate the Nu_{max} value on the rotor surface when $(r/D) > 1$. The location of this maximum value appear to be only a function of the dimensionless spacing interval G. The following law can thus be obtained:

$$(r/D)_{max} = 3\,[1 - 0.76\,exp(-25\,G)] \tag{12}$$

When G is high, the jet at the pipe outlet is more widely spread, thus the radius of the maximum local Nusselt number is also greater.

By observing the mean Nusselt numbers, the effect of the cooling technique on the whole rotor can be determined. Optimizing this cooling technique requires a compromise between all the parameters. In the next section, the laws concerning the mean Nusselt numbers $\overline{Nu}$ are highlighted.

4.4.2 Mean Nusselt numbers

To allow the influence of the rotation or the jet to be seen more easily, correlations for the mean Nusselt numbers were sought. For narrow dimensionless spacing intervals ($0.01 \leq G \leq 0.02$), the following law was obtained:

$$\overline{Nu} = 0.08\,G^{-0.07}\,Re_j^{0.5}\,Re^{0.25} \tag{13}$$

For wide intervals, two divisions were made in order to best represent the global heat transfers at the rotor surface. When $0.04 \leq G \leq 0.08$:

$$\overline{Nu} = 0.006\,G^{0.15}\,Re_j^{0.5}\,Re^{0.5} \tag{14}$$

And when $G = 0.16$,

$$\overline{Nu} = 0.06\,Re_j^{0.25}\,Re^{0.5} \tag{15}$$

For the three ranges, as G increases, the power of Re_j decreases, whereas the power of Re increases. This highlights the fact that, for low G values, the flow is essentially centrifugal and the heat transfers are influenced by the jet. When the G values are higher, the influence of rotation is dominant over the mean Nusselt number. Figure 10 presents a comparison of the correlated results and some experimental data.

5 Conclusion

This article has examined the influence of a jet on the convective heat transfers on a rotor surface in a discoidal system. Our heat transfer measurements confirm the data about flow structure published in the literature. The observed increase in the local heat transfers is more significant in the central area, near the stagnation point, where the jet influence is preponderant. For higher radii, the experimental convective heat transfers are similar to those obtained without a jet. Given that similarity, it was possible to identify three zones on the disk surface and to correlate the separations between those zones. In our range of parameters, adding a jet is always advantageous for the heat transfers. Power laws were used to correlate the mean Nusselt numbers on the rotor surface as functions of G, Re and Re_j, highlighting the influence of each parameter. The addition of a jet impinging the center of the rotor is advantageous for the heat transfers, primarily near the stagnation point. In order to complete this research and to further improve the cooling at outer radii, a study with several impinging jets added at positive radii could be done.

References

[1] T. Von Karman. ber laminar und turbulente reibung. *Math. Mech.*, 1, pp. 244–252, 1921.

[2] S. Goldstein. Dans *Cambridge Phil. soc.*, volume 31, page 232, 1935.

[3] E.C. Cobb et O.A. Saunders. Heat transfer from a rotating disk. Dans *Proc. Roy. Soc. A.*, volume 236, pages 343–351, 1956.

[4] P.D. Richardson et O.A. Saunders. Studies of flow and heat transfer associated with a rotating disk. *J. Mech. eng. SC.5*, 4, pp. 336–342, 1963.

[5] L.A. Dorfman. *Hydrodynamic resistance and heat loss from rotating solids.* Edinburgh and London, 1963.

[6] G. Cardone, T. Astarita, et G.M. Carlomagno. Infrared heat transfer measurements on a rotating disk. *Optical Diagnostics in Engineering*, 1, pp. 1–7, 1996.

[7] L. Huang et M.S. El-Genk. Heat transfer and flow visualization experiments of swirling, multi-channel, and conventional impinging jets. *Int. J. Heat and Mass Transfer*, 41, pp. 583 – 600, 1998.

[8] M. Fenot, J.J. Vullierme, et E. Dorignac. Local heat transfer due to several configurations of circular air jets impinging on a flat plate with and without semi-confinement. *Int. J. of Thermal Sciences*, 44, pp. 665–675, 2005.

[9] M. Angioletti, R.M. Di Tommaso, E. Nino, et G. Ruocco. Simultaneous visualization of flow field and evaluation of local heat transfer by transitionnal impinging jets. *Heat and Mass Transfer*, 46, pp. 1703–1713, 2003.

[10] Y.M. Chen, W.T. Lee, et S.J. Wu. Heat (mass) transfer between an impinging jet and a rotating disk. *Heat and Mass Transfer*, 34, pp. 195–201, 1998.

[11] J.M. Owen et M.H. Rogers. *Flow and Heat Transfer in rotating disk systems*, volume 1 of *Rotor-stator systems*. 1989.

[12] T. Astarita et G. Cardone. Convective heat transfer on a rotating disk with a centred impinging round jet. *Int. J. of Heat and Mass Transfer*, 51, pp. 1562–1572, 2008.

[13] C.Y. Soong, C.C. Wu, Tung-Ping Liu, et Tao-Ping Liu. Flow structure between two co-axial disks rotating independently. *Exp. Thermal and Fluid Science*, 27, pp. 295–311, 2003.

[14] C.O. Popiel et L. Boguslawski. Numerical modeling of heat transfer and fluid flow in rotorstator cavities with throughflow. *Inter. J. Heat and Mass Transfer*, 50, pp. 1528–1544, 2007.

[15] G.P. Beretta et E. Malfa. Flow and heat transfer in cavities between rotor and stator disks. *Int. J. Heat and Mass Transfer*, 46, pp. 2715–2726, 2003.

[16] J. Pelle et S. Harmand. Heat transfer measurements in an opened rotor stator system air gap. *Experimental Thermal and Fluid Sciences*, 31, pp. 165–180, 2007.

[17] S.L. Soo. Laminar flow over an enclosed rotating disk. *Trans. ASME*, 80, pp. 287–296, 1959.

[18] K. Stewartson. On the flow between two rotating coaxial disks. Dans *Camb. Phil. Soc.*, volume 49, pages 333–341, 1953.

[19] Ritoux G. Evaluation numrique des facteurs de forme. *Revue Phys. Appl.*, 17, pp. 503–515, 1982.

[20] C.O. Popiel et L. Boguslawski. Local heat transfer from a rotating disk in an impinging round jet. *J. of Heat Transfer*, 108, pp. 357–364, 1986.

[21] J.X. Chen, X. Gan, et J.M. Owen. Heat transfer in an air-cooled system. *Journal of Turbomachinery*, 118, pp. 444–451, 1996.

[22] G.K. Batchelor. Note on a class of solutions of the navier-stokes equations representing steady rotationnally-symmetric flow. *Quart. J. Mech.; Appl. Math.*, 5, pp. 29–41, 1951.

List of Figures

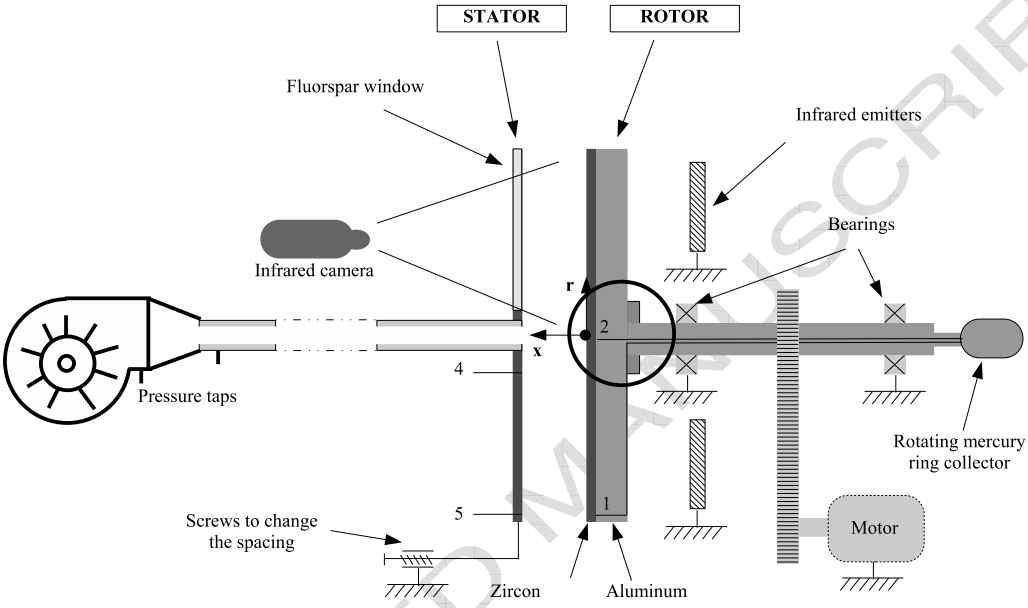

Fig. 1. Experimental Set-up

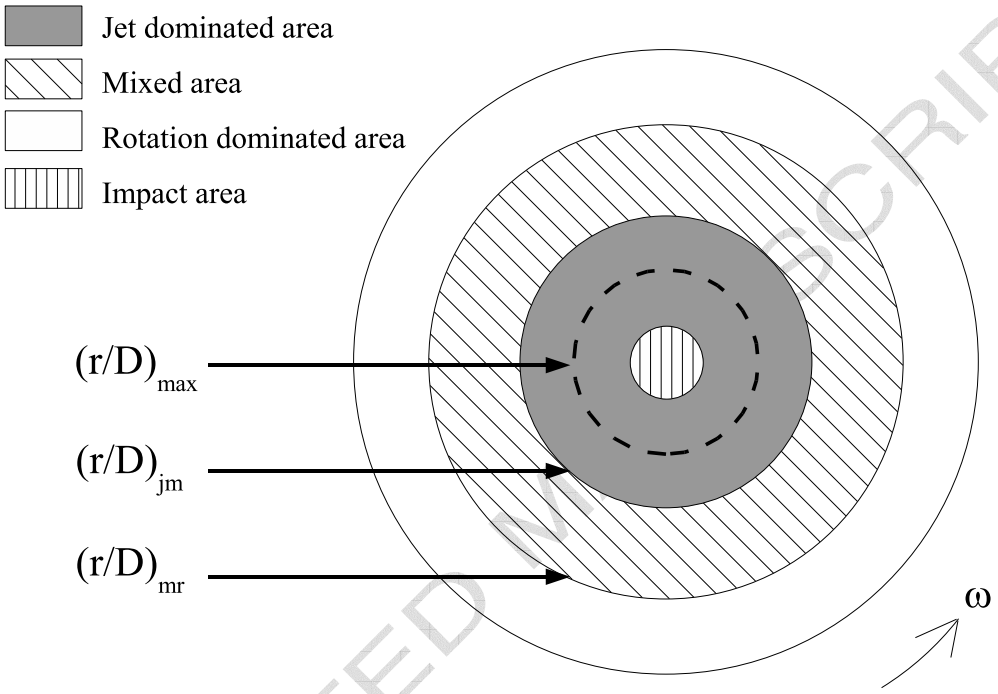

Fig. 2. Phenomena at the rotor surface - Correlated parameters

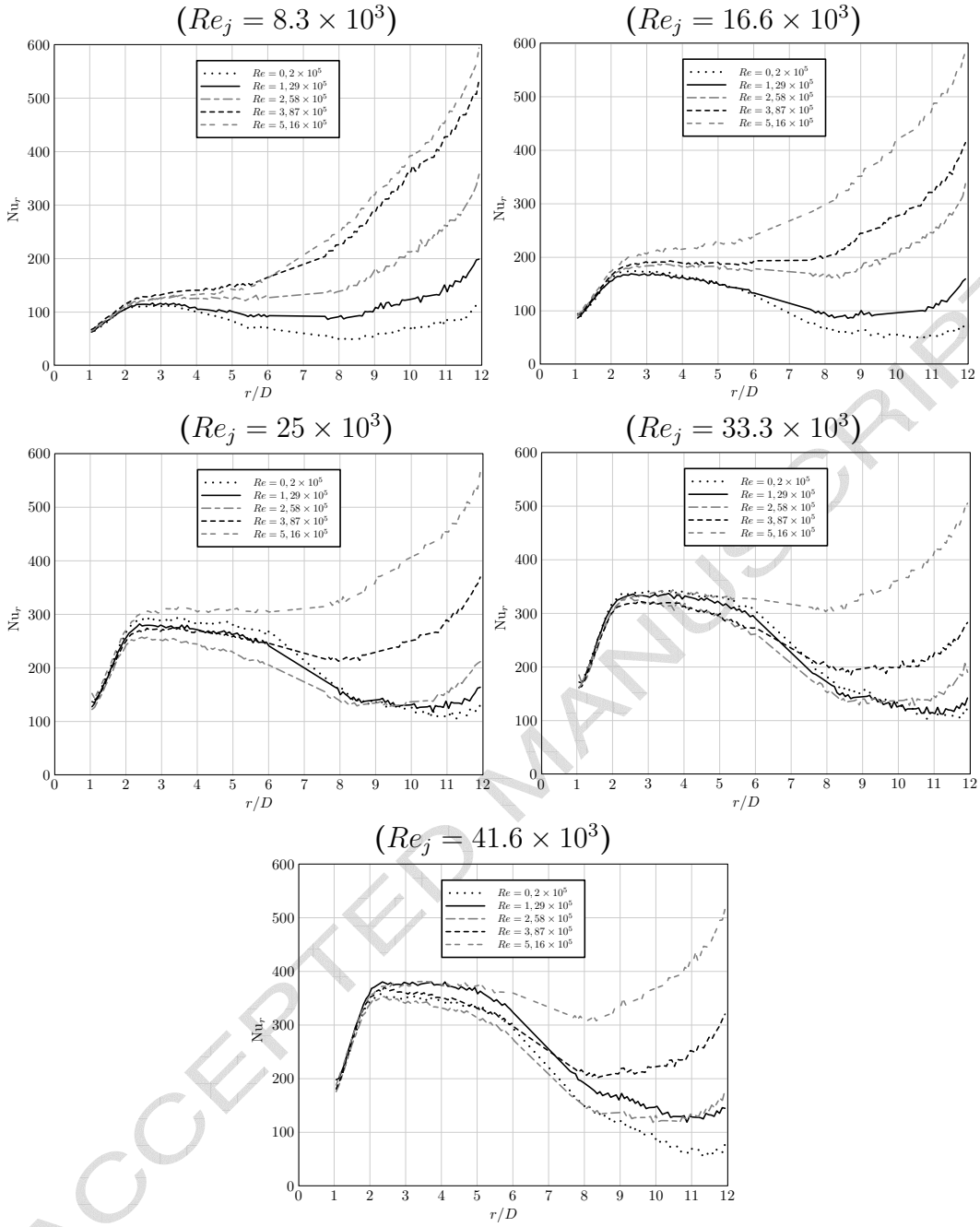

Fig. 3. Local Nusselt numbers for $G = 0.16$ and for different Re_j

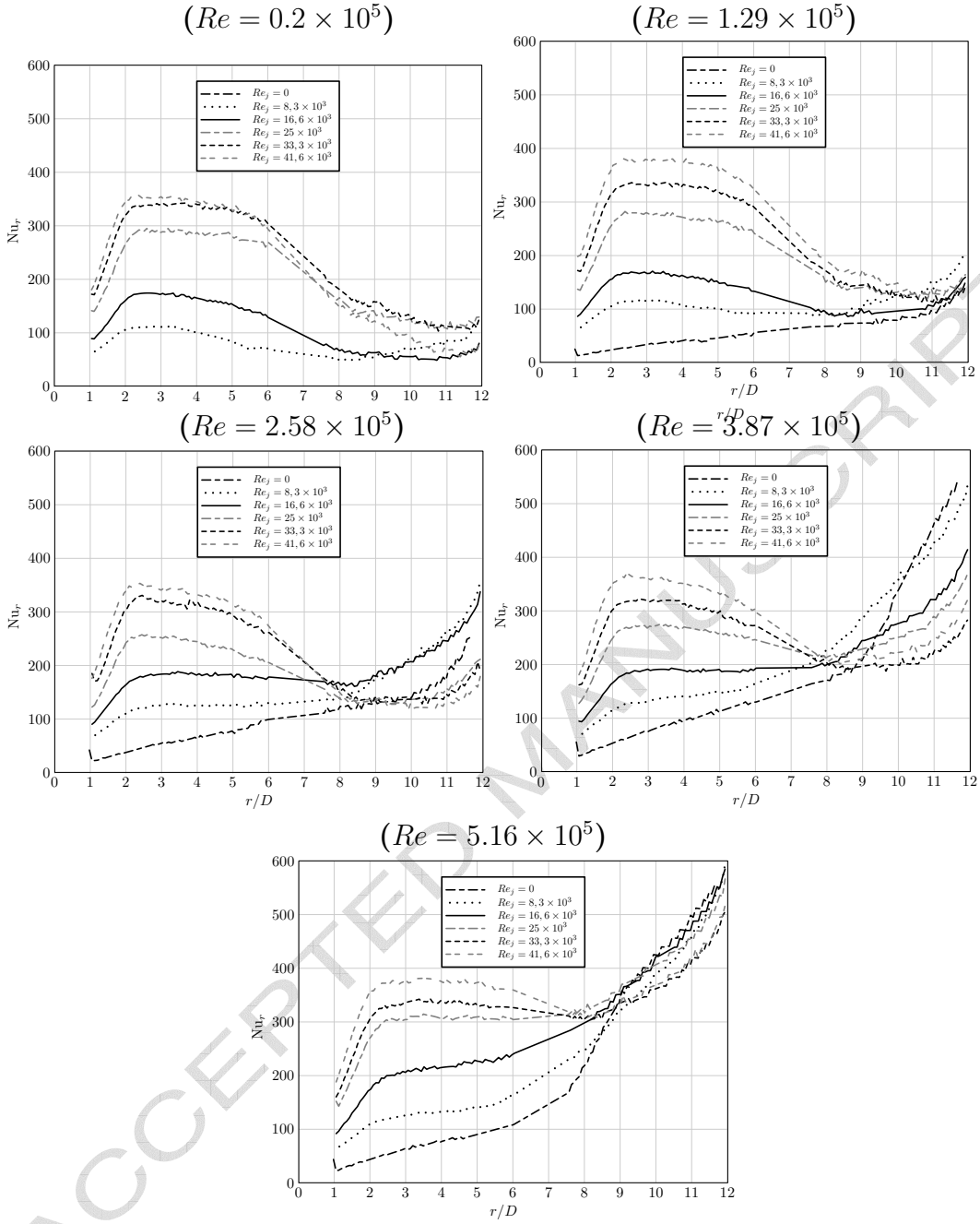

Fig. 4. Local Nusselt numbers for $G = 0.16$ and for different Re

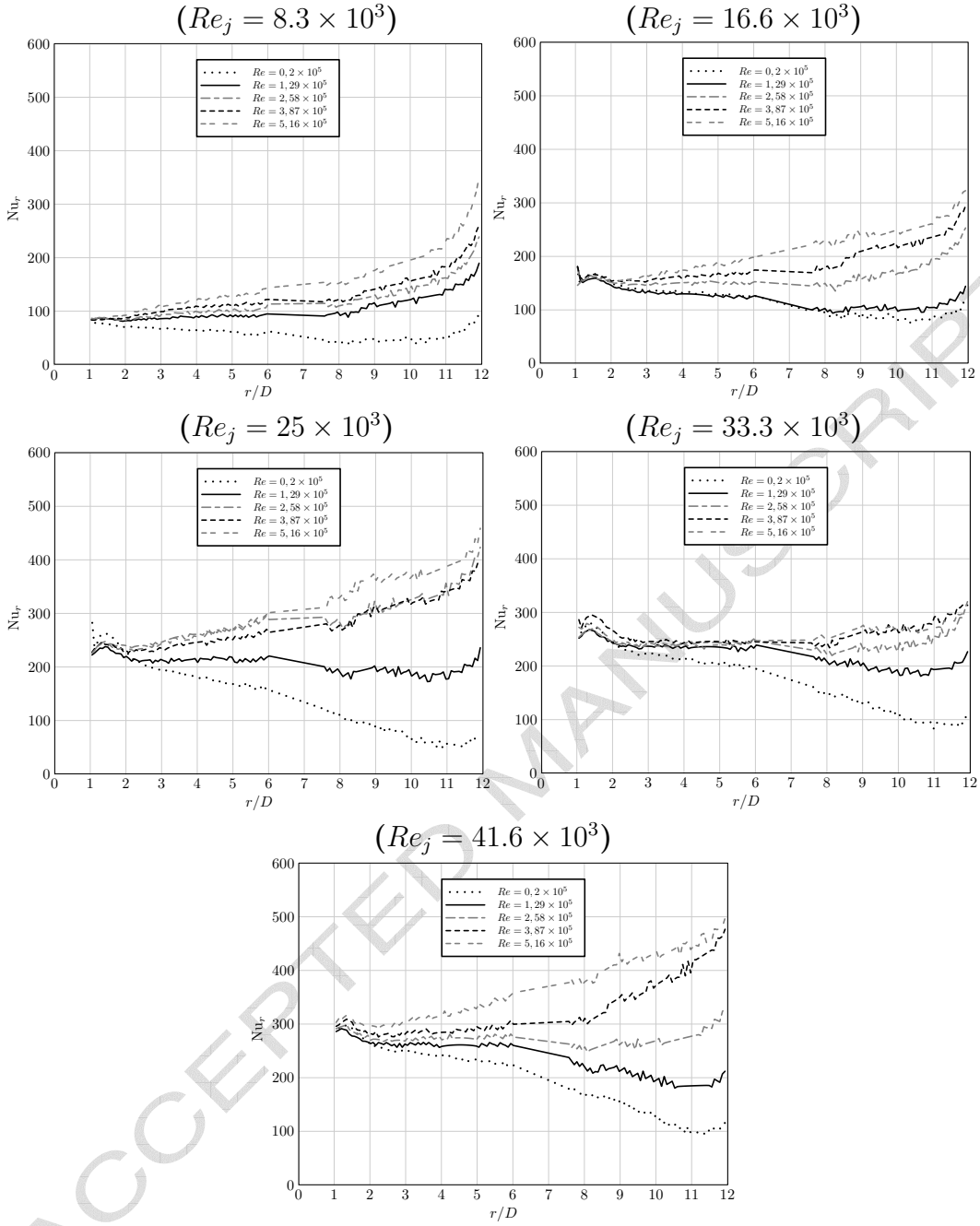

Fig. 5. Local Nusselt numbers for $G = 0.01$ and for different Re_j

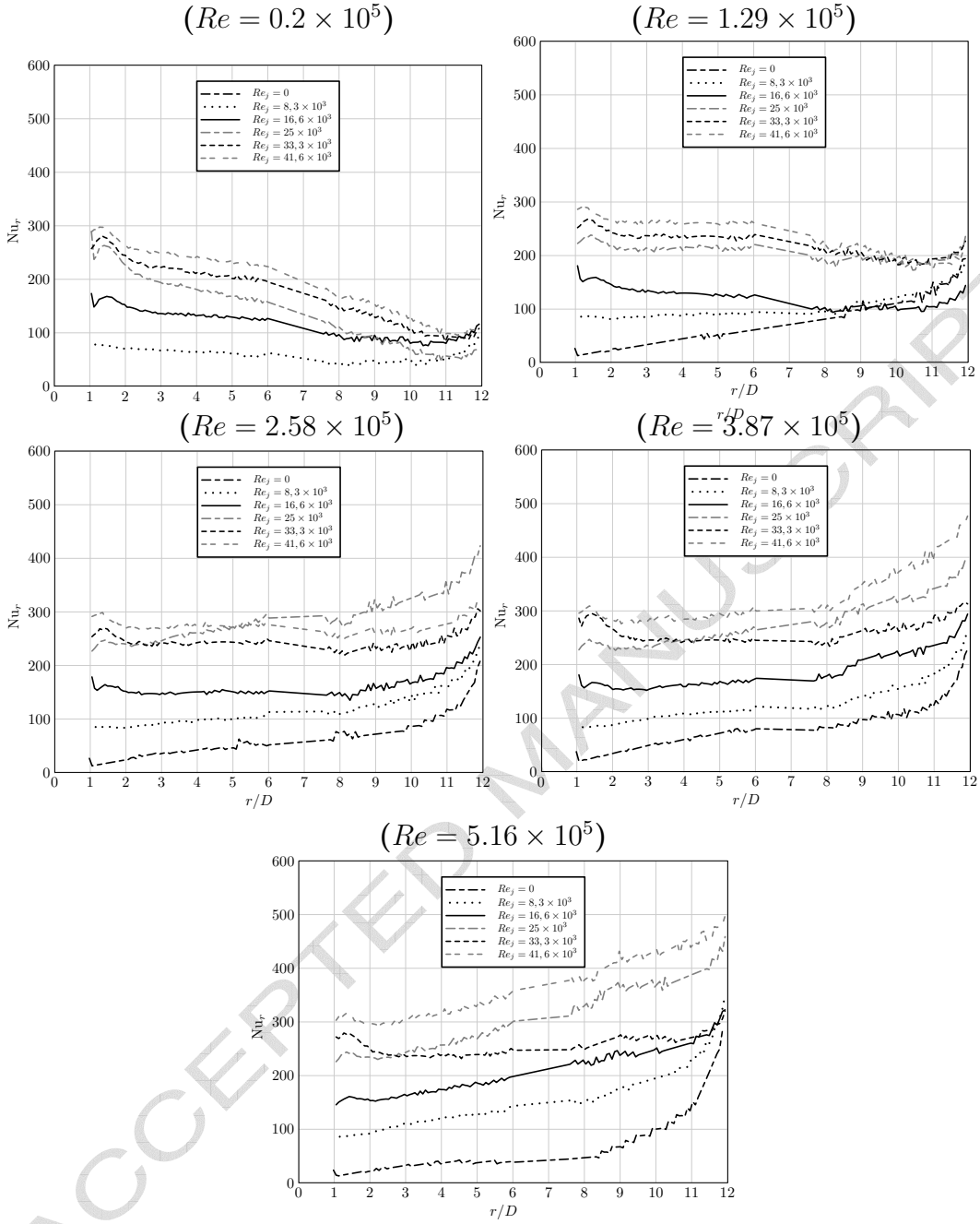

Fig. 6. Local Nusselt numbers for $G = 0.01$ and for different Re

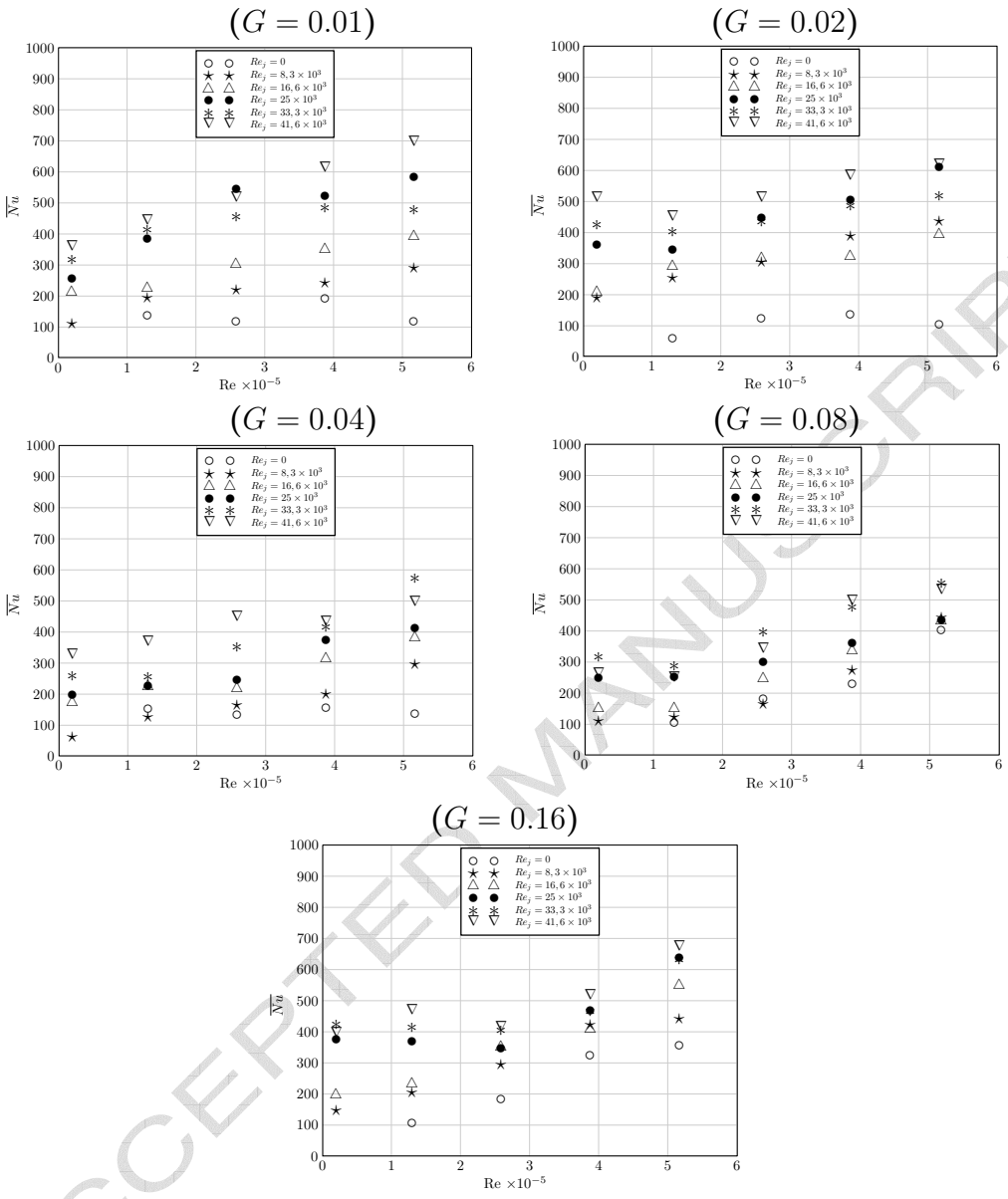

Fig. 7. Mean Nusselt numbers for different G; Influence of Re

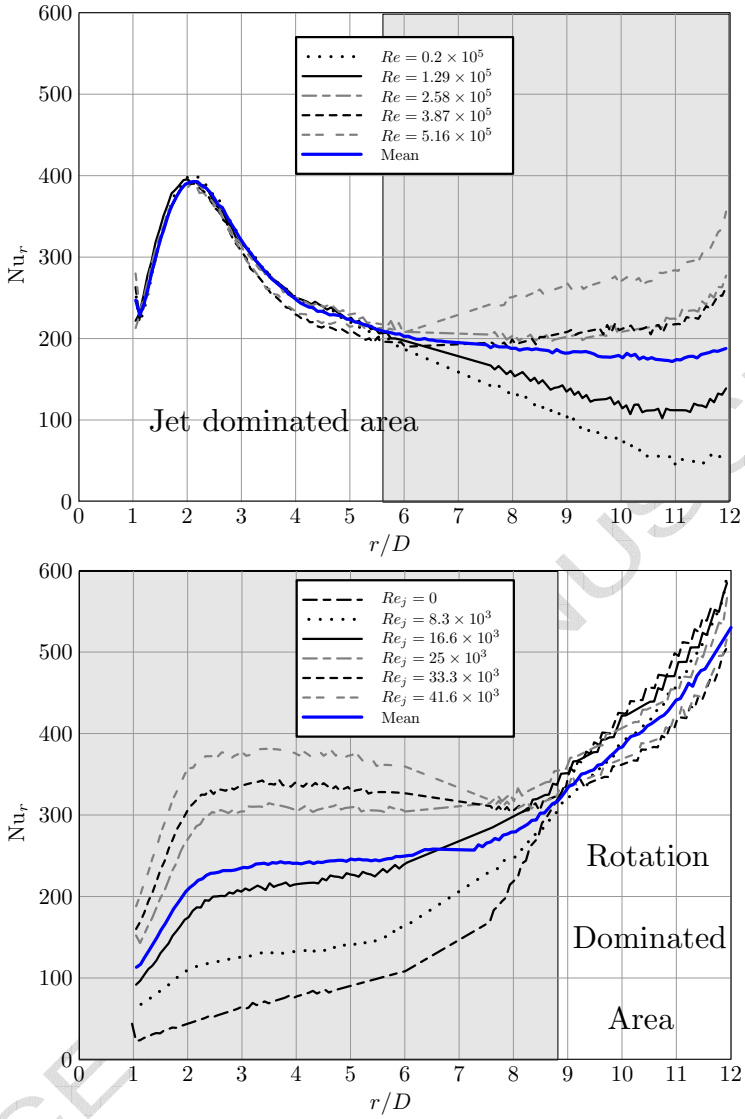

Fig. 8. Identification method of the limits between the three regimes - *Top:* $G = 0.04$ *and* $Re_j = 41.6 \times 10^3$ - *Bottom:* $G = 0.16$ *and* $Re = 5.16 \times 10^5$

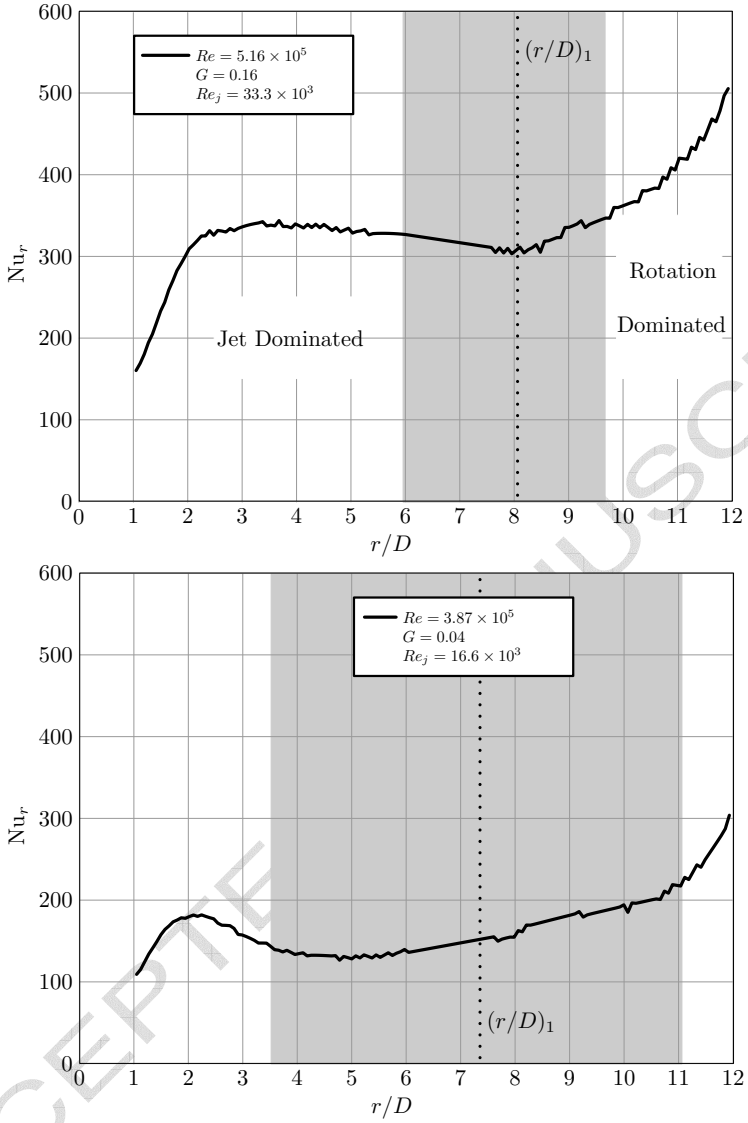

Fig. 9. Concordance between heat transfers and flows in two cases

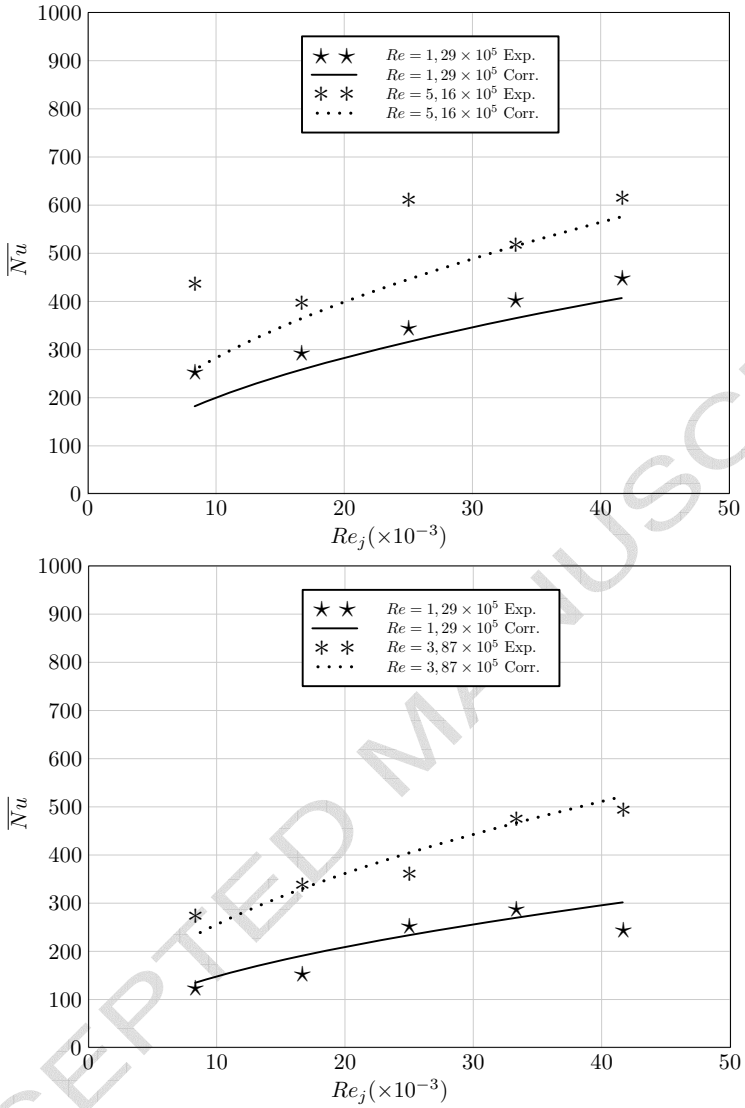

Fig. 10. Comparison between experimental and correlated data in several cases - *Top:* $G = 0.02$ - *Bottom:* $G = 0.08$